

RESEARCH

Open Access



Protein arginine deiminase 2 (PAD2) modulates the polarization of THP-1 macrophages to the anti-inflammatory M2 phenotype

Aneta Stachowicz^{1,2}, Rakhi Pandey², Niveda Sundararaman³, Vidya Venkatraman³, Jennifer E. Van Eyk^{2,3} and Justyna Fert-Bober^{2*}

Abstract

Background: Macrophages are effector cells of the innate immune system that undergo phenotypical changes in response to organ injury and repair. These cells are most often classified as proinflammatory M1 and anti-inflammatory M2 macrophages. Protein arginine deiminase (PAD), which catalyses the irreversible conversion of protein-bound arginine into citrulline, is expressed in macrophages. However, the substrates of PAD and its role in immune cells remain unclear. This study aimed to investigate the role of PAD in THP-1 macrophage polarization to the M1 and M2 phenotypes and identify the citrullinated proteins and modified arginines that are associated with this biological switch using mass spectrometry.

Results: Our study showed that PAD2 and, to a lesser extent, PAD1 and PAD4 were predominantly expressed in M1 macrophages. We showed that inhibiting PAD expression with BB-CI-amidine decreased macrophage polarization to the M1 phenotype (TNF- α , IL-6) and increased macrophage polarization to the M2 phenotype (MRC1, ALOX15). This process was mediated by the downregulation of proteins involved in the NF- κ B pathway. Silencing PAD2 confirmed the activation of M2 macrophages by increasing the antiviral innate immune response and interferon signalling. A total of 192 novel citrullination sites associated with inflammation, cell death and DNA/RNA processing pathways were identified in M1 and M2 macrophages.

Conclusions: We showed that inhibiting PAD activity using a pharmacological inhibitor or silencing PAD2 with PAD2 siRNA shifted the activation of macrophages towards the M2 phenotype, which can be crucial for designing novel macrophage-mediated therapeutic strategies. We revealed a major citrullinated proteome and its rearrangement following macrophage polarization, which after further validation could lead to significant clinical benefits for the treatment of inflammation and autoimmune diseases.

Keywords: Citrullination, Protein arginine deiminases, Proteomics, Macrophage polarization, Posttranslational modifications

Background

The protein arginine deiminase (PAD) family of enzymes catalyses the conversion of positively charged arginine residues within a protein to neutrally charged citrulline in a hydrolytic reaction termed citrullination

*Correspondence: Justyna.Fert-Bober@cshs.org

² Advanced Clinical Biosystems Research Institute, Smidt Heart Institute, Cedars-Sinai Medical Center, CA, Los Angeles, USA
Full list of author information is available at the end of the article



© The Author(s) 2022. **Open Access** This article is licensed under a Creative Commons Attribution 4.0 International License, which permits use, sharing, adaptation, distribution and reproduction in any medium or format, as long as you give appropriate credit to the original author(s) and the source, provide a link to the Creative Commons licence, and indicate if changes were made. The images or other third party material in this article are included in the article's Creative Commons licence, unless indicated otherwise in a credit line to the material. If material is not included in the article's Creative Commons licence and your intended use is not permitted by statutory regulation or exceeds the permitted use, you will need to obtain permission directly from the copyright holder. To view a copy of this licence, visit <http://creativecommons.org/licenses/by/4.0/>. The Creative Commons Public Domain Dedication waiver (<http://creativecommons.org/publicdomain/zero/1.0/>) applies to the data made available in this article, unless otherwise stated in a credit line to the data.

or deamination [1, 2]. This irreversible reaction has attracted attention due to its involvement in various physiologic and pathologic conditions [3, 4]. On the global level PAD isoforms have been reported to be widespread in inflammatory cells [5, 6]. It has been shown that the activation of PAD4 in neutrophils triggers histone citrullination and chromatin decondensation, resulting in neutrophil extracellular trap (NET) formation during host defence, inflammation, and autoimmunity [7]. Similarly, PAD2 has been shown to mediate macrophage NETosis (ETosis or METosis) [8] and pyroptosis, an inflammatory form of macrophage death [9]. Notably, it has been shown that PAD2 may be involved in THP-1 monocyte differentiation to macrophages [10]; however, neither the role of PAD in macrophage polarization to proinflammatory and anti-inflammatory phenotypes nor the proteins that are specifically citrullinated have been investigated.

Macrophages play a pivotal role in innate immunity and are involved in the development of low-grade chronic inflammation in many disorders, such as atherosclerosis [11], rheumatoid arthritis [12] and Alzheimer's disease [13]. Tissue-resident macrophages are very plastic and can be classified according to two main phenotypes: proinflammatory M1 macrophages (classically activated) and anti-inflammatory M2 macrophages (alternatively activated). M1 macrophages emerge in response to lipopolysaccharide (LPS) and interferon gamma (IFN- γ), while M2 macrophages are generated in response to interleukin-4 (IL-4) and interleukin-13 (IL-13) [14]. In general, M1 macrophages are characterized by the production of nitric oxide (NO) and inflammatory cytokines (i.e., interleukin-1 beta (IL-1 β), tumour necrosis factor α (TNF- α), and interleukin-6 (IL-6)) and are responsible for the clearance of pathogens, whereas M2 macrophages release anti-inflammatory cytokines and play a role in the resolution of inflammation, tissue repair and wound healing [15, 16]. Notably, macrophage class switching from proinflammatory M1 to anti-inflammatory M2 cells could be a potential therapeutic target in the treatment of chronic inflammatory diseases [17].

Thus, we aimed to investigate the role of PAD during THP-1 macrophage polarization to proinflammatory M1 and anti-inflammatory M2 phenotypes. Furthermore, we aimed to determine the citrullinated proteins and modified arginines that are associated with this biological switch using mass spectrometry. Revealing the major citrullinated proteome and its rearrangement following macrophage polarization could lead to significant clinical benefits for the treatment of inflammation and autoimmune diseases.

Results

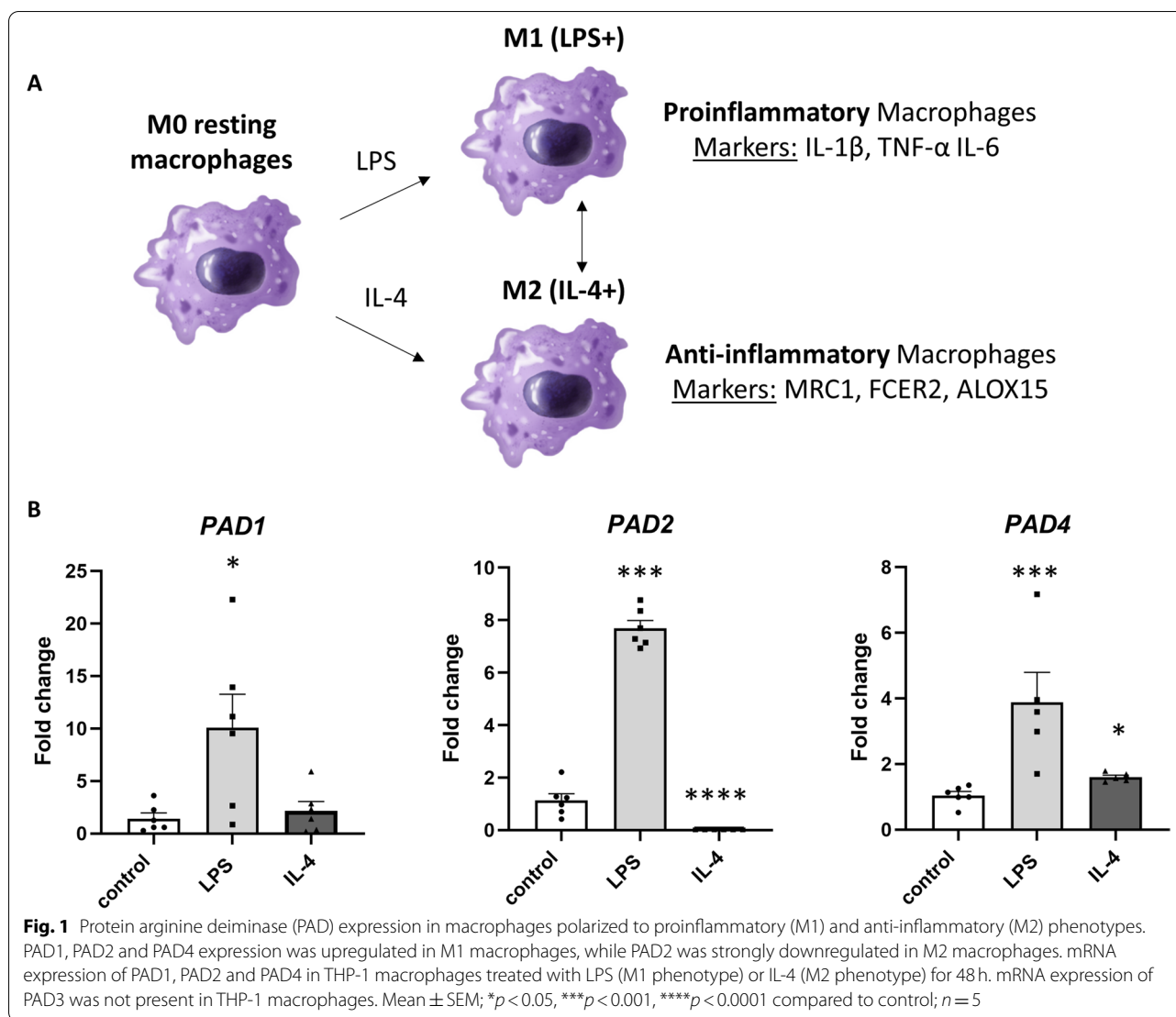
PAD2 is the most abundant PAD isoform in THP-1 macrophages

In this study, differently polarized human THP-1 macrophages were analyzed by quantitative proteomics to evaluate PAD role during macrophage polarization. We first investigated the polarization of THP-1 macrophages to proinflammatory and anti-inflammatory phenotypes as presented in Fig. 1A. We then focused on the PAD1, PAD2, PAD3 and PAD4 mRNA expression levels that were measured by quantitative RT-PCR. The most abundant PAD isoforms in resting THP-1 macrophages (control) were PAD2 (cycle threshold (Ct)=25.87 \pm 0.16) and PAD1 (Ct=31.06 \pm 0.33), followed by PAD4 (Ct=35.47 \pm 0.21). We did not detect any mRNA expression of PAD3. PAD expression was altered in proinflammatory and anti-inflammatory THP-1 macrophages. We observed statistically significant increases in PAD1 (fold change (FC)=10.06 \pm 3.19 vs. FC=1.43 \pm 0.52 in control, p <0.05), PAD2 (FC=7.7 \pm 0.3 vs. FC=1.14 \pm 0.25 in control, p <0.001), and PAD4 (FC=3.34 \pm 0.92 vs. FC=1.04 \pm 0.12 in control, p <0.001) mRNA expression levels in LPS-treated macrophages (proinflammatory M1 type). Interestingly, the mRNA expression of PAD2 (FC=0.0299 \pm 0.0007 vs. FC=1.14 \pm 0.25 in control, p <0.0001) was highly downregulated in IL-4-treated THP-1 macrophages (anti-inflammatory M2 type), while the mRNA expression of PAD4 (FC=1.47 \pm 0.14 vs. FC=1.04 \pm 0.12 in control, p <0.05) was upregulated (Fig. 1B).

The pan-PAD inhibitor – BB-Cl-amidine decreases the polarization of THP-1 macrophages to the M1 phenotype and increases polarization to the M2 phenotype

The mRNA expression of PAD1, PAD2 and PAD4 differed between proinflammatory and anti-inflammatory THP-1 macrophages and was particularly upregulated in proinflammatory M1 cells. To determine whether PAD activation affects the switch in THP-1 macrophages to the M1 and M2 phenotypes, we used BB-Cl-amidine, which irreversibly inhibits the activity of all PADs [18]. In our experiments, we chose a dose of BB-Cl-amidine equal to 100 nM based on the results of the MTT cell viability assay (Fig. 2 E).

BB-Cl-amidine treatment of THP-1 macrophages significantly reduced the mRNA expression of proinflammatory markers, such as TNF- α (FC=7.64 \pm 0.4 vs. FC=8.43 \pm 0.4 in LPS-treated cells, p <0.05) and IL-6 (FC=29.41 \pm 3.61 vs. FC=49.75 \pm 3.95 in LPS-treated cells, p <0.01) in M1 cells (Fig. 2A) and upregulated the mRNA expression of anti-inflammatory markers, including MRC1



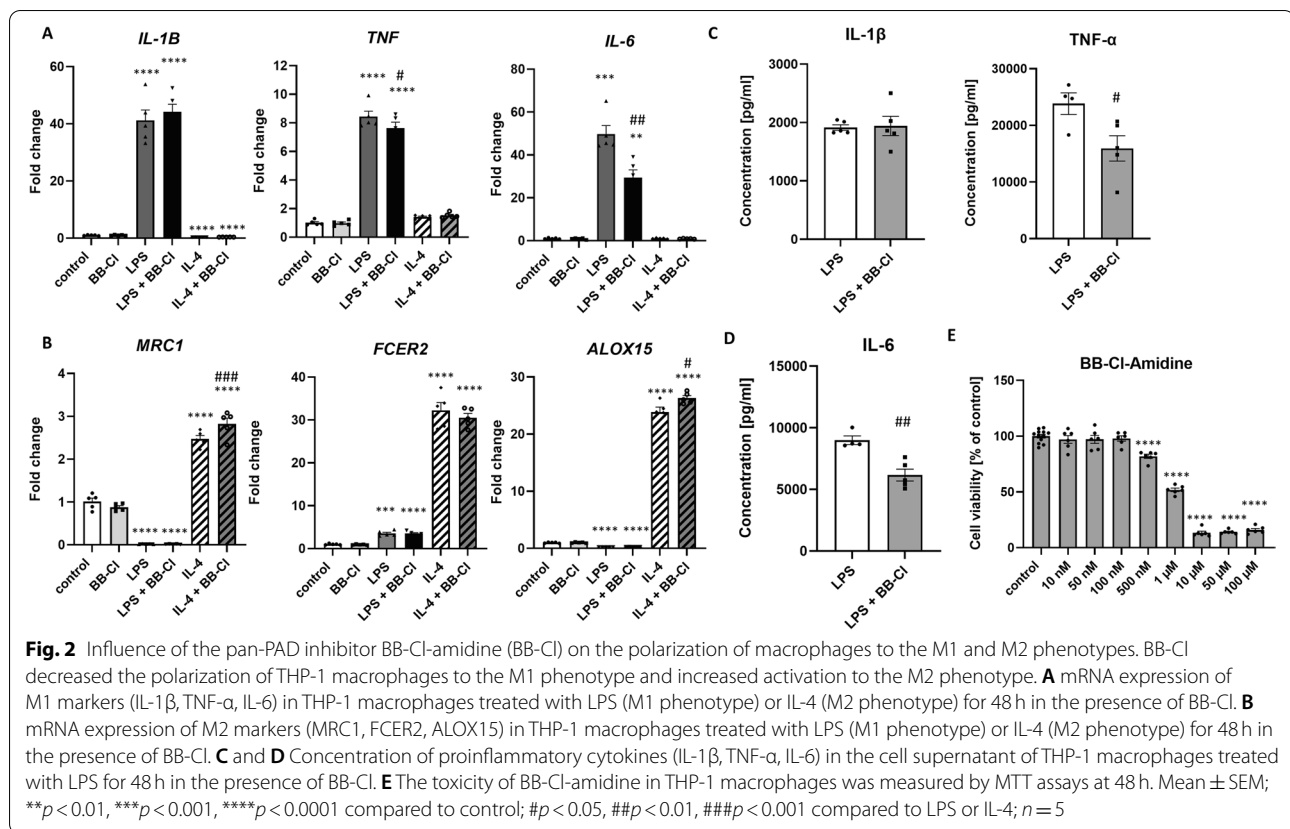
(FC = 2.82 ± 0.13 vs. FC = 2.47 ± 0.08 in IL-4-treated cells, $p < 0.001$) and ALOX15 (FC = 26.31 ± 0.43 vs. FC = 23.86 ± 0.87 in IL-4-treated cells, $p < 0.05$), in M2 cells (Fig. 2B). Furthermore, the levels of the proinflammatory cytokines TNF- α ($15,928 \pm 2240$ vs. $23,835 \pm 1912$ in LPS-treated cells, $p < 0.05$) and IL-6 (6164 ± 483 vs. 8993 ± 346 in LPS-treated cells, $p < 0.01$) were decreased in the cell supernatant of M1 macrophages after treatment with BB-Cl-amidine (Fig. 2C and D).

Inhibition of PAD activity alters proinflammatory pathways in THP-1 macrophages

In vitro experiments showed that inhibiting PAD activity in THP-1 macrophages (BB-Cl-amidine treatment) decreased the switch in macrophages to the M1 type and augmented polarization to the M2 type. To further

understand the mechanism involved and identify relevant citrullinated proteins, we analysed the proteomic profile of M1 and M2 cell lysates by MS.

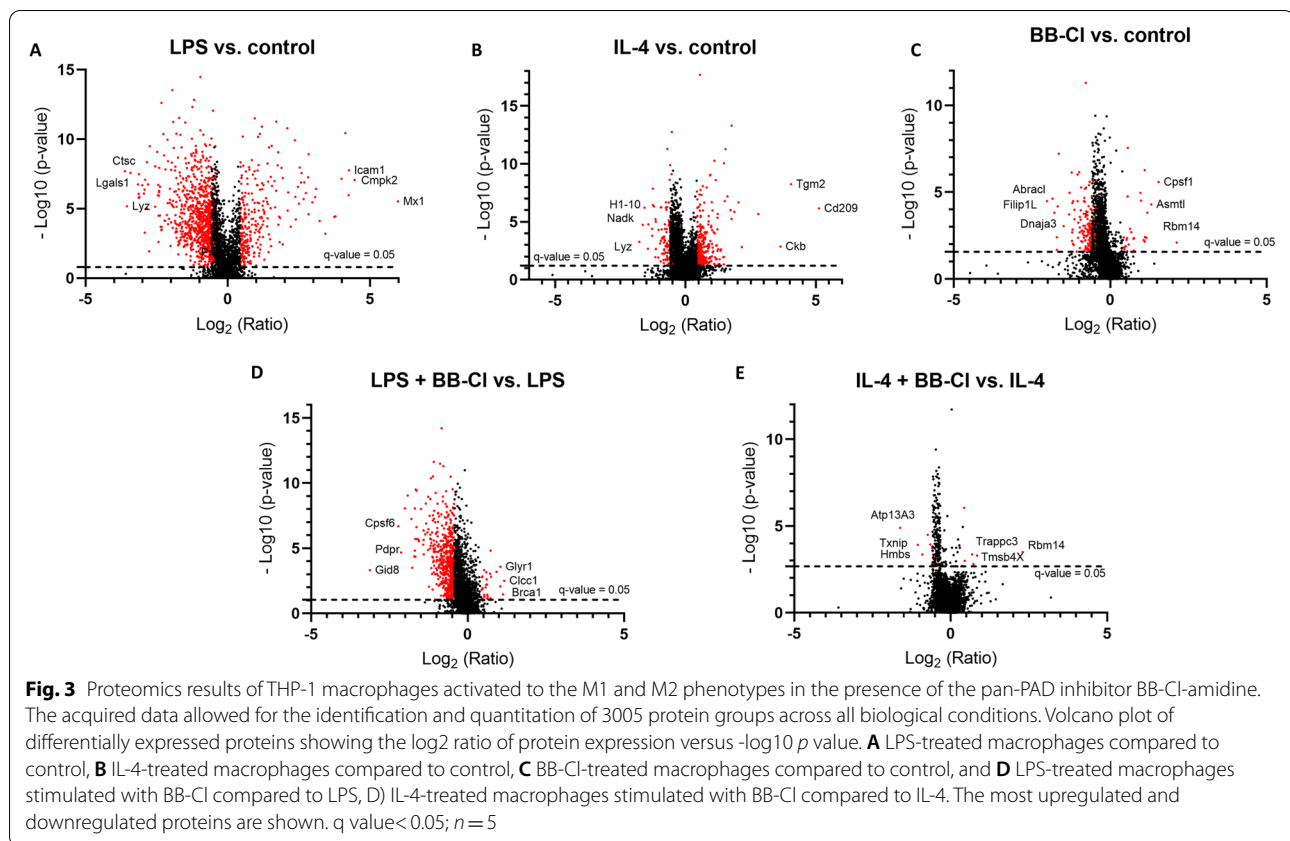
Liquid chromatography – tandem mass spectrometry (LC-MS/MS) measurements operated in DDA mode identified 22,211 peptides, providing a macrophages spectral library composed of 4832 protein groups. The obtained library was used to analyse DIA runs in Spectronaut. Spectral library recovery was 85%, and the median protein group CV was approximately 20% (Supplemental Fig. 1), which allowed for the calculation of a significant cut-off equal to a fold change of 1.35 (statistical power greater than 80%). A summary of the quality control for the LC-MS/MS runs is shown in Supplemental Fig. 1.



The acquired data allowed for the identification and quantitation of 3005 protein groups across all biological conditions. A total of 254 proteins were altered in BB-Cl-amidine-treated THP-1 macrophages compared to the control; 1160 proteins were altered in LPS-stimulated cells compared to control as well as 435 proteins were differentially expressed in IL-4 stimulated macrophages in comparison to the control (Fig. 3). BB-Cl-amidine administration to proinflammatory M1 macrophages (LPS stimulated) led to 554 differentially expressed proteins compared to LPS-treated cells, while only 24 proteins were altered in anti-inflammatory M2 macrophages (IL-4 stimulated) treated with BB-Cl-amidine in comparison to IL-4-treated macrophages (Fig. 3). Using cut-offs of $q < 0.05$ and $\log_2 FC \leq 0.433$, we found decreased levels of several proteins, including NF-kappa-B essential modulator (IKBKG), protein kinase C beta type (PRKCB), inhibitor of nuclear factor kappa-B kinase subunit beta (IKK2), ubiquitin-conjugating enzyme E2 variant 1 (UBE2V1), interferon-induced 35 kDa protein (IFI35), mitochondrial antiviral-signalling protein (MAVS), double-stranded RNA-activated protein kinase (EIF2AK2) and receptor-interacting serine/threonine-protein kinase 1 (RIPK1) (Fig. 4A). Furthermore, we observed decreased expression of stimulator of interferon genes protein (STING1)

in proinflammatory M1 and anti-inflammatory M2 macrophages after treatment with BB-Cl-amidine (FC = -1.92 and -1.42, respectively) (Supplemental Table 1). In M2 macrophages, the administration of BB-Cl-amidine did not result in statistically significant changes in protein expression, except thioredoxin-interacting protein (TXNIP) (FC = -2.07) and caspase-1 (FC = -1.51), which were downregulated in M2 macrophages after BB-Cl administration (Supplemental Table 1).

Moreover, the expression levels of proteins that participate in oxidative phosphorylation - respiratory electron transport in mitochondria were diminished in BB-Cl-amidine-treated and LPS-stimulated macrophages (Fig. 4A). Interestingly, this effect was not reflected in the functional analysis of mitochondria, as we did not detect differences in the OCR in M1 and M2 macrophages treated with BB-Cl-amidine (Fig. 4B). The detailed list of differentially expressed proteins and their fold changes across all biological conditions are presented in Supplemental Table 1. Additionally, enriched pathway analyses performed by PINE on M1 (LPS+) and M2 (IL-4+) macrophages are depicted in Supplemental Fig. 2.



Silencing PAD2 in THP-1 macrophages increases the activation of macrophages to the M2 phenotype

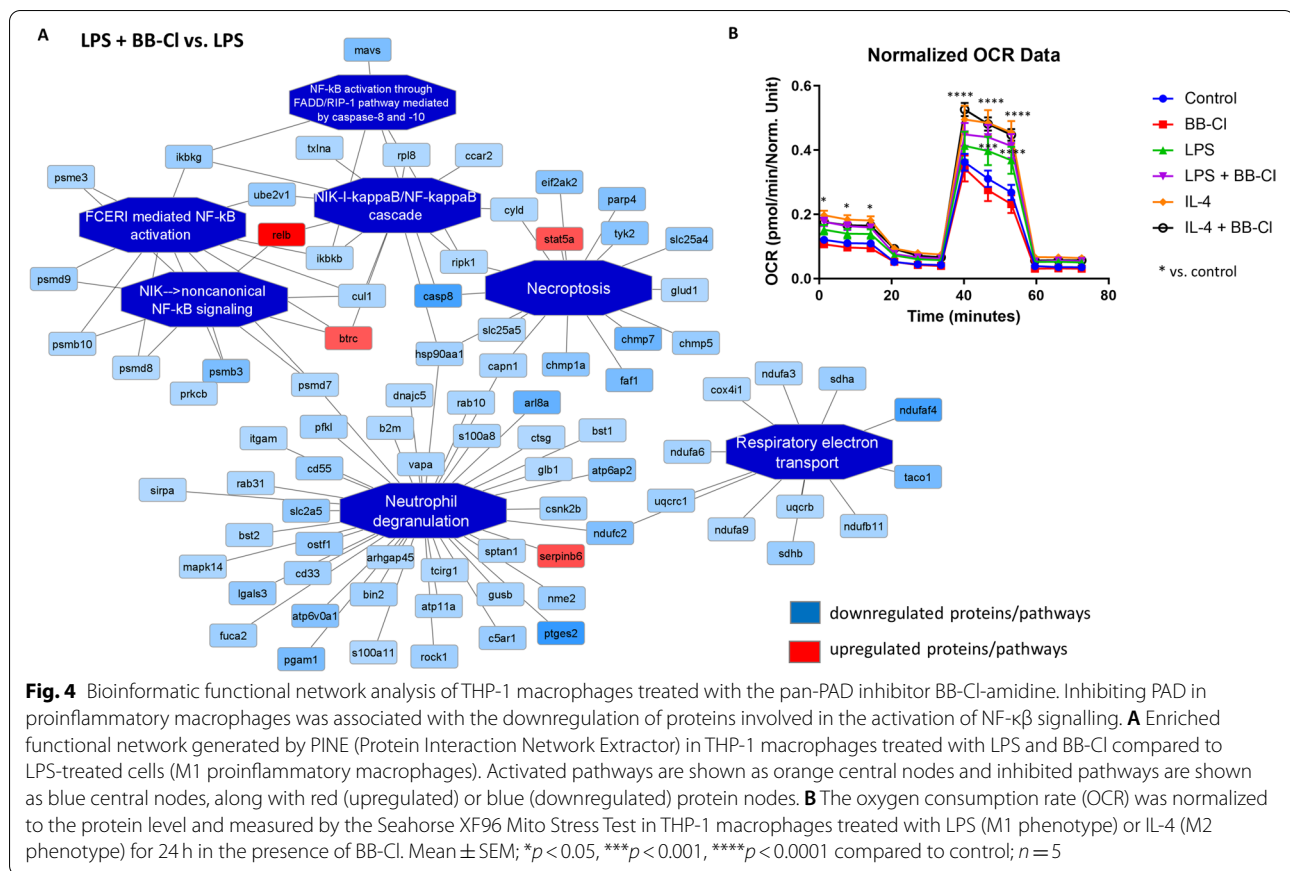
To further understand the mechanism by which PAD modulates macrophages polarization, we silenced PAD2 in macrophages, since PAD2 was the most highly expressed PAD isozyme in THP-1 macrophages. We confirmed the silencing of PAD2 (siPAD2) in control, LPS-treated and IL-4-treated macrophages by real-time PCR (Fig. 5D). PAD2 silencing did not influence the mRNA expression of PAD4, but PAD1 mRNA expression tended to be increased (FC = 2.42 ± 1.36 vs. FC = 0.61 ± 0.19 in siCON + LPS-treated cells, *p* > 0.05; FC = 3.98 ± 2.19 vs. FC = 0.31 ± 0.13 in siCON + IL-4-treated cells, *p* < 0.05) in comparison to cells treated with the scrambled siRNA control (siCON) and stimulated with either LPS or IL-4 (Fig. 5E). This result might reflect the compensatory role of PAD1 in THP-1 macrophages with silenced PAD2.

Silencing PAD2 in LPS-stimulated proinflammatory macrophages did not change the mRNA expression of the proinflammatory markers IL-1β and TNF-α (Fig. 5A). However, it increased the mRNA expression of IL-6 (FC = 2.79 ± 0.51 vs. FC = 0.7 ± 0.1 in siCON + IL-4-treated cells, *p* < 0.05) in M2 macrophages and tended to upregulate IL-6 expression in M1 macrophages (FC = 2.06 ± 0.46 vs. FC = 1.16 ± 0.17 in siCON

+ LPS-treated cells, *p* > 0.05) (Fig. 5A). This trend was also confirmed by ELISA analysis of the supernatant of LPS-stimulated THP-1 macrophages treated with siPAD2 (97.01 ± 8.03 vs. 28.56 ± 3.28 in siCON + LPS-treated cells, *p* < 0.001) (Fig. 5C). Interestingly, silencing PAD2 upregulated the mRNA expression of anti-inflammatory markers of M2 macrophages, including MRC1 (FC = 3.81 ± 0.28 vs. FC = 2.15 ± 0.16 in siCON + IL-4-treated cells, *p* < 0.001; FC = 1.24 ± 0.13 vs. FC = 1.03 ± 0.11 in siCON cells, *p* < 0.05), FCER2 (FC = 41.12 ± 3.60 vs. FC = 26.19 ± 3.86 in siCON + IL-4-treated cells, *p* < 0.01; FC = 2.08 ± 0.32 vs. FC = 1.08 ± 0.18 in siCON cells, *p* < 0.05), and ALOX15 (FC = 13.29 ± 1.08 vs. FC = 10.57 ± 1.24 in siCON + IL-4-treated cells, *p* < 0.05; FC = 1.43 ± 0.16 vs. FC = 1.02 ± 0.09 in siCON cells, *p* < 0.01) in both control cells and IL-4 stimulated macrophages (Fig. 5B).

Silencing PAD2 in THP-1 macrophages upregulates pathways related to interferon signalling

MS analysis after silencing PAD2 in THP-1 macrophages identified 3820 protein groups across all biological conditions. Using cut-offs of *q* < 0.05 and log₂FC ≤ 0.322, we found 205 proteins that were altered in THP-1 macrophages with silenced PAD2 compared to scrambled

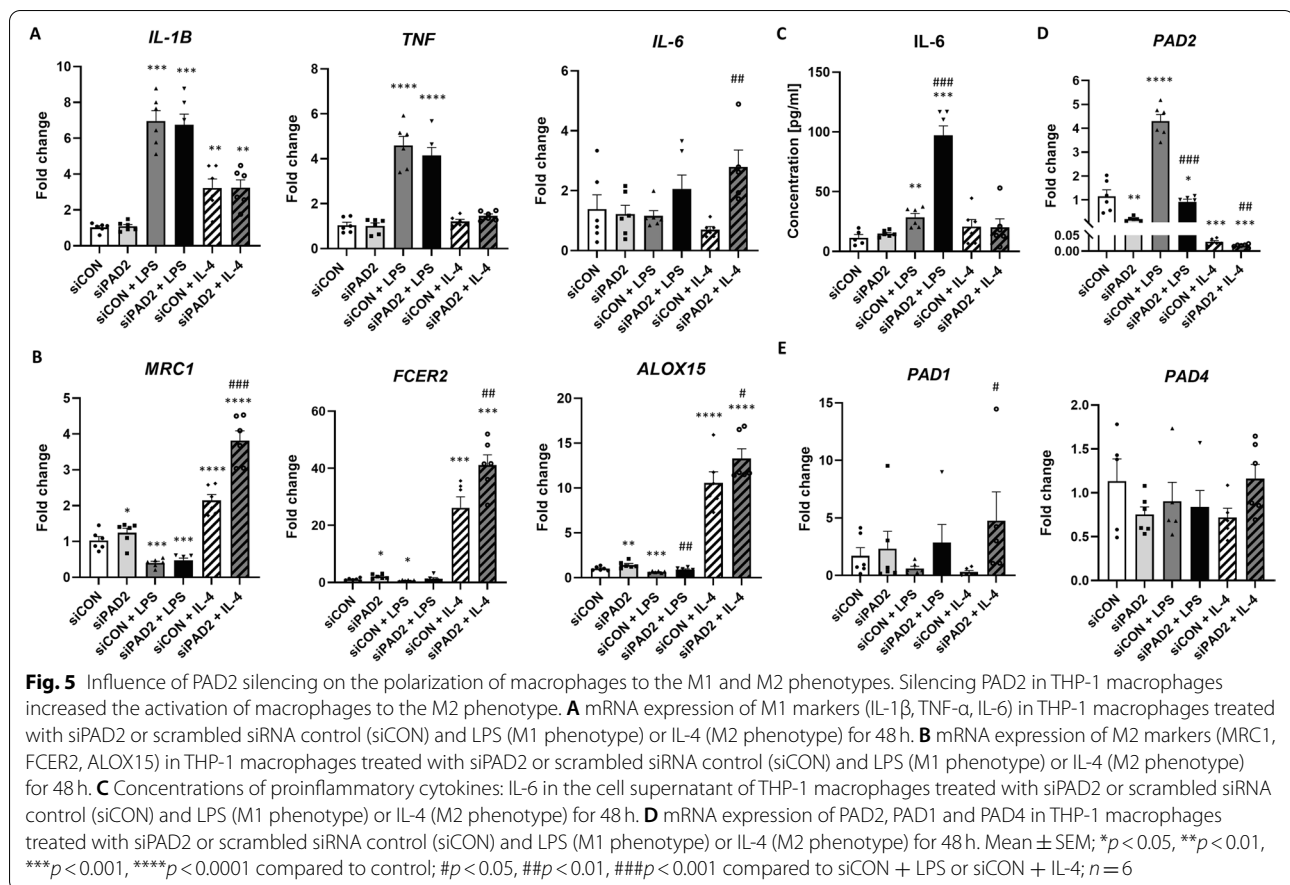


siRNA control cells and 306 proteins that were differentially expressed in LPS-stimulated, PAD2-silenced cells in comparison to LPS-stimulated, scrambled siRNA-treated control macrophages (Fig. 6A and B). The detailed list of differentially expressed proteins and their fold changes across all biological conditions are presented in Supplemental Table 2. The summary of quality control for LC-MS/MS runs is presented in Supplemental Fig. 3. Enriched pathway analysis showed the upregulation of interferon signalling, DNA replication and the cell cycle in PAD2-silenced THP-1 macrophages (Fig. 6C and D). Furthermore, proteins responsible for the antiviral innate immune response and interferon signalling, such as the interferon-induced GTP-binding proteins Mx1 and Mx2 (MX1 and MX2); 2'-5'-oligoadenylate synthases 1, 2 and 3 (OAS1, OAS2 and OAS3); interferon-induced transmembrane protein 3 (IFITM3); ubiquitin-like protein ISG15 (ISG15); bone marrow stromal antigen 2 (BST2) and the antiviral innate immune response receptor RIG-I (DDX58 or RIG-I), were increased in PAD2-silenced cells. Furthermore, our study revealed that in PAD2-silenced macrophages, the expression of HLA class II histocompatibility antigen gamma chain (CD74)

was upregulated (FC = 2.1) in comparison to scrambled siRNA control cells (Supplemental Table 2).

Protein citrullination landscape of THP-1 macrophages

To confirm whether PAD activation was necessary and sufficient for THP-1 polarization, we next identified the citrullinated targets of PAD. Using mass spectrometry analysis based on a hypercitrullinated library, we identified 192 citrullinated sites, 180 citrullinated peptides and 152 citrullinated proteins in THP-1 macrophages (Supplemental Table 3A). We identified a modest 21 citrullinated peptides and proteins in BB-Cl-treated THP-1 macrophages polarized to the M1 and M2 phenotypes (Supplemental Table 3A), whereas in PAD2-silenced macrophages, we identified 66 citrullinated peptides and 61 citrullinated proteins (Supplemental Table 3B). The identified and quantified citrullinated proteins in THP-1 macrophages were engaged in signalling by interleukins, neutrophil degranulation, programmed cell death, DNA and RNA processing, proteasomal degradation, platelet activation and VEGF signalling, among others (Fig. 7C). The expression levels of some citrullinated peptides were significantly different between biological conditions, including X-ray repair cross-complementing protein 6



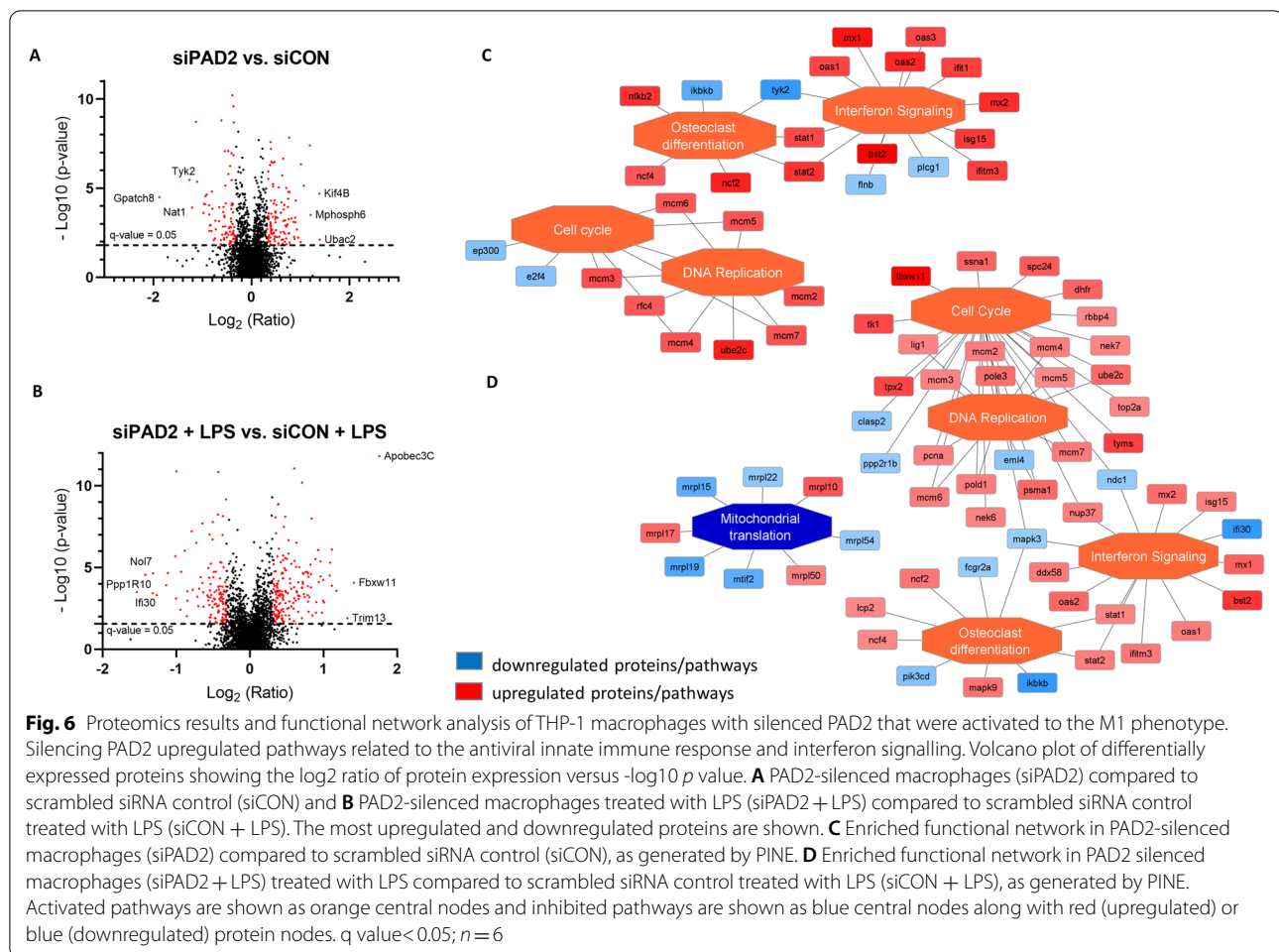
(XRCC6 or Ku70), plectin, small nuclear ribonucleoprotein Sm D2 (SNRPD2) and alpha-2-HS-glycoprotein (AHSG or fetuin-A) (Fig. 7A, B, D and E, respectively). The citrullination of Ku70 on arginine 115 (R115) was downregulated, whereas the citrullination of plectin on arginine 3039 (R3039) was upregulated in LPS-treated proinflammatory THP-1 macrophages (Fig. 7A and B). Furthermore, the citrullination of SNRPD2 on arginine 47 (R47) was decreased, and the citrullination of fetuin-A on arginine 143 (R143) was increased in PAD2-silenced macrophages (Fig. 7D and E).

Discussion

PADs are a group of hydrolase enzymes expressed in immune cells, and PAD4 and PAD2 are primarily expressed at high levels in neutrophils, monocytes, and macrophages [5, 6]. Although both isoforms are involved in the regulation of inflammatory processes within immune cells, including ETosis in neutrophils [7] and macrophages [8] and pyroptosis mediated by NLRP3 inflammasome activation [9], the detailed mechanism has not been investigated. To address this gap, the THP-1 monocytic cell line was differentiated into macrophages

in vitro and then further activated to the M1 or M2 phenotype. The mRNA expression of PAD1, PAD2 and PAD4 was detected in THP-1 macrophages, and PAD2 was the most abundant isoform. Importantly, PAD2 was highly upregulated in M1 macrophages but strongly downregulated in M2 macrophages. Notably, PAD1 and PAD4 were also upregulated in proinflammatory M1 macrophages. Furthermore, for the first time, we reported that PAD modulates the polarization of THP-1 macrophages to proinflammatory M1 and anti-inflammatory M2 phenotypes.

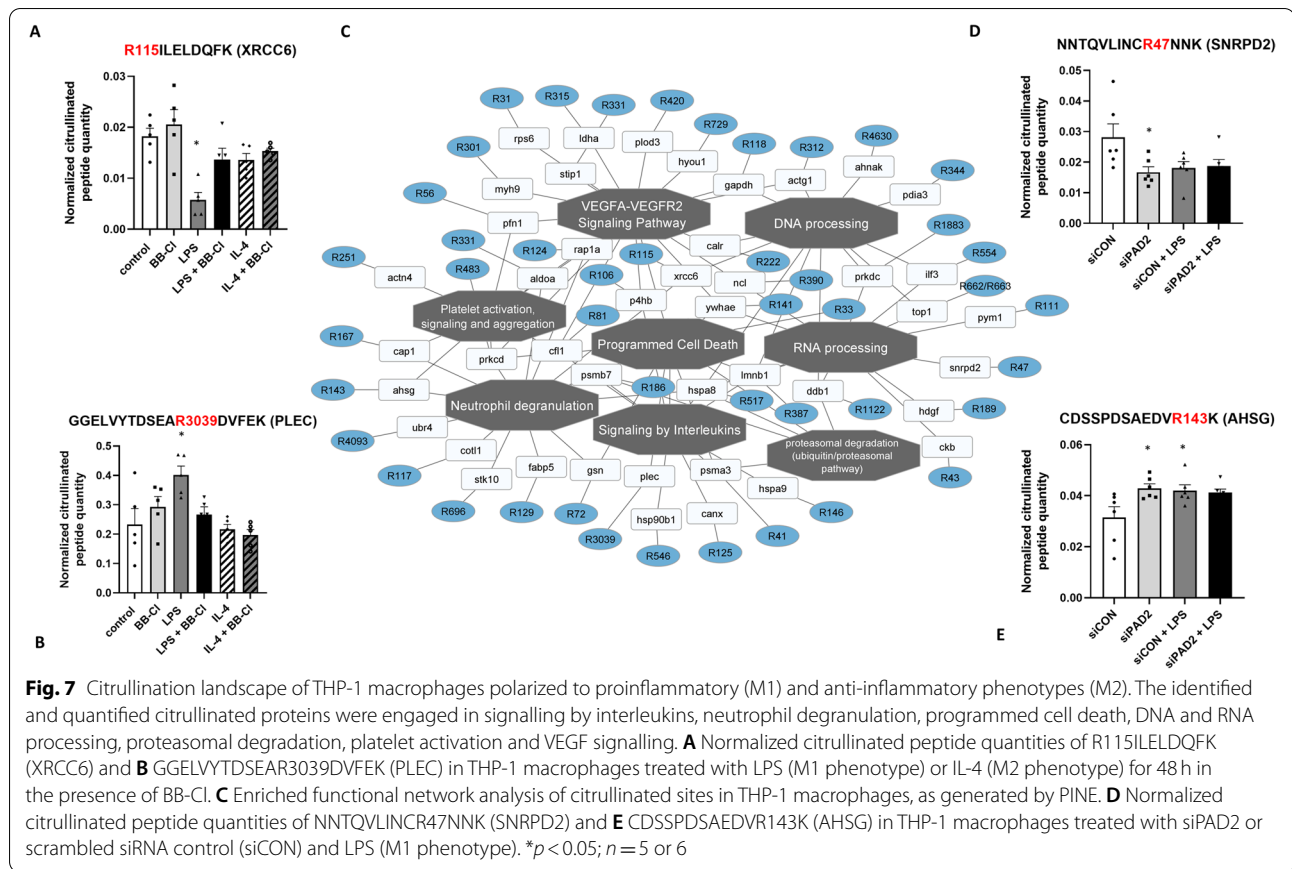
Our results further showed that PAD inhibition decreased proinflammatory M1 markers (TNF- α and IL-6) and increased anti-inflammatory M2 markers (MRC1 and ALOX15) in THP-1 macrophages stimulated with LPS or IL-4. We did not observe decreased levels of IL-1 β in the supernatant of LPS-stimulated THP-1 macrophages, which suggests that in our experiments, BB-CI-amidine did not block NLRP3 inflammasome activation. This finding is contrary to Mishra et al., which showed the blockage of NLRP3 inflammasome activation and IL-1 β release after inhibiting PAD activity with Cl-amidine in bone marrow-derived macrophages (BMDMs)



[9]. We hypothesize that these differences could be explained by the use of PAD inhibitors that are stronger and less susceptible to proteolysis, a different cell line or a different method of macrophage differentiation. Herein, we reported that inhibiting PAD expression in proinflammatory THP-1 macrophages was associated with the downregulation of several proteins involved in the activation of NF- κ B, such as IKBKG, PRKCB, IKK2, UBE2V1, IFI35, MAVS, EIF2AK2 and RIPK1 (Fig. 4A) [19–26], as determined by DIA-MS proteomic methods. NF- κ B is a rapid-acting transcription factor that plays an important role in regulating the immune response to infection and the production of proinflammatory cytokines [27]. NF- κ B is constantly active in many chronic inflammatory diseases [28]. Moreover, RIPK1 is a key regulator of necroptosis and promotes the production of the proinflammatory cytokines IL-6 and TNF- α [29]. Importantly, BB-Cl-amidine administration decreased the expression of IL-6 and TNF- α at both the mRNA and protein levels in proinflammatory M1 macrophages, which may be associated with the downregulation of RIPK expression.

Furthermore, we observed decreased expression of STING1 in both M1 and M2 macrophages after treatment with the PAD inhibitor BB-Cl-amidine. STING promotes the production of type I interferon and activates several transcription factors, such as NF- κ B [30]. STING also contributes to the proinflammatory M1-like macrophage profile by stabilizing HIF-1 α , which enhances glycolysis, NOS production and inflammasome activation [31].

Notably, inhibiting PAD with BB-Cl-amidine increased the M2 polarization of macrophages. This effect was related to the downregulation of TXNIP and caspase-1 expression. TXNIP activates the NLRP3 inflammasome and can facilitate M1 polarization but might inhibit M2 polarization [32]. In turn, caspase-1 is responsible for IL-1 β and IL-18 production as well as pyroptosis induction [33]. Decreased protein expression of TXNIP and caspase-1 in BB-Cl-amidine-treated, IL-4-stimulated macrophages favours the activation of THP-1 macrophages towards an anti-inflammatory phenotype. Based on these findings, we hypothesize



that the inhibition of PAD activity alters the M1 phenotype by downregulating NF- κ B pathway and favours M2 polarization. It is tempting to hypothesize that BB-Cl-amidine is a potential therapeutic agent for treating chronic inflammatory diseases.

To test our hypothesis, PAD2 in THP-1 macrophages was silenced by siRNA. Silencing PAD2 upregulated the mRNA expression of anti-inflammatory markers characteristic of the M2 phenotype (MRC1, FCER2, ALOX15) in both control cells and IL-4-stimulated THP-1 macrophages. Interestingly, silencing PAD2 did not change the mRNA expression of the proinflammatory markers IL-1 β and TNF- α , except for IL-6 expression. In our study, the level of IL-6 in the supernatant of proinflammatory M1 macrophages increased. This might be a result of NF- κ B activation, as it has been previously shown that PAD2 suppresses NF- κ B activity by interacting with IKK γ , an essential regulatory subunit of the I κ B kinase complex [34]. Our results contradict those of Yu et al., who demonstrated the promotion of IL-1 β , IL-6 and TNF- α production in U937 macrophages with *Pad2* knockout [6]; however, the cell types, cell origin and methodology cannot be

directly compared, which suggests dynamic regulation of PAD isoforms, and potentially citrullination.

Furthermore, our data suggest that PAD2 regulates THP-1 macrophage polarization to the anti-inflammatory M2 phenotype, which may explain the low expression levels of PAD2 in M2 macrophages. Notably, silencing PAD2 in THP-1 macrophages upregulated pathways related to the antiviral innate immune response and interferon signalling. MX1, MX2, OAS1, OAS2, OAS3, IFITM3, ISG15, BST2 and RIG-I levels were increased in PAD2-silenced cells. Interestingly, RIG-I, which is a sensor of cytoplasmic viral nucleic acids and leads to the generation of type I interferons when activated, was also found to be involved in IL-6 production [35]. Moreover, silencing PAD2 augmented the level of IL-6 in LPS-treated THP-1 macrophages. BB-Cl-amidine treatment of THP-1 macrophages decreased proteins involved in interferon signalling, which is consistent with other studies showing a decrease in the expression of type I interferon-regulated genes in response to BB-Cl-amidine administration in a systemic lupus erythematosus mouse model [5]. Thus, further investigations are needed to elucidate the role of PAD2 and other PAD isoforms in anti-viral innate immune responses and interferon signalling.

Herein, we demonstrated that PAD2 was involved in the regulation of anti-inflammatory M2 macrophages, which was associated with the upregulation of CD74 expression. CD74 is a cell surface receptor for the immunomodulatory cytokine macrophage migration inhibitory factor (MIF), which plays a role in the regulation of macrophage function. It has been shown that MIF-CD74 activation is important for IL-4-induced M2 macrophage polarization in malignant diseases and parasitic infection through the TLR4-PI3K-Akt pathway [36–38]. However, other studies have shown contradictory effects of MIF on the induction of M1 macrophage polarization [39]. In our study, silencing PAD2 or pharmacological inhibition of PAD isoforms in M1 macrophages led to the upregulation of the MIF receptor CD74. In contrast, LPS stimulation caused the downregulation of CD74 expression in THP-1 proinflammatory M1 macrophages (Supplemental Tables 1 and 2). Whether the increase in CD74 protein expression is related to PAD2 inhibition and involved in the polarization of macrophages to the M2 phenotype requires further investigation.

Importantly, we first identified 192 citrullinated sites on 180 citrullinated peptides corresponding to 152 citrullinated proteins in M1 and M2 THP-1 macrophages using a hypercitrullinated library approach combined with DIA-based LC-MS/MS. The identified and quantified citrullinated proteins are involved in signalling by interleukins, neutrophil degranulation, programmed cell death, DNA and RNA processing, proteasomal degradation, platelet activation and VEGF signalling (Fig. 7). The expression levels of some citrullinated proteins, including Ku70 (XRCC6), plectin (PLEC), small nuclear ribonucleoprotein Sm D2 (SNRPD2), and fetuin-A (AHSG), were different between biological conditions. Ku70 is a single-stranded DNA-dependent ATP-dependent helicase that participates in double-strand break repair, chromosome translocation and activation of the innate immune system [40]. Interestingly, it has been observed that Ku70 and Ku80 promote LPS-induced NF- κ B activation and proinflammatory cytokine production in human macrophages and monocytes [41]. In our study, citrullinated Ku70 (R115) levels were downregulated in LPS-stimulated THP-1 macrophages. In turn, citrullinated plectin (R3039) was increased in LPS-treated proinflammatory macrophages. Plectin is an important component of the cytoskeleton; it responds to mechanical forces and interlinks intermediate filaments with microtubules [42]. Notably, citrullination of cytoskeletal proteins such as vimentin, fibrin, collagen II and filaggrin has been reported in various autoimmune diseases [3]. It has been shown that citrullination of cytoskeletal proteins has functional consequences on cell physiology; for example, the citrullination of collagen II affects integrin-mediated

cell adhesion [43], and the citrullination of vimentin mediates the development and progression of lung fibrosis [44].

Our results also indicated the increased citrullination of fetuin-A (R143) in PAD2-silenced macrophages. Fetuin-A is a circulating glycoprotein produced by liver and adipose tissue. It acts as a chemoattractant for macrophage infiltration into adipose tissue and the conversion of macrophages to the M1 phenotype [45]. Recent evidence indicates that fetuin-A is a crucial factor that modulates tissue inflammation and fibrosis, as well as a systemic indicator of acute inflammatory disease [46]. Interestingly, several studies have demonstrated an association between fetuin-A serum levels and rheumatoid arthritis disease activity [47]; however, a direct link between the citrullinated form of fetuin A and rheumatoid arthritis has never been presented. The small nuclear ribonucleoprotein Sm D2 belongs to the small nuclear ribonucleoprotein core protein family. It plays pivotal roles in pre-mRNA splicing as a core component of spliceosomal U1, U2, U4 and U5 small nuclear ribonucleoproteins (snRNPs), which are the building blocks of the spliceosome [48]. Importantly, proteins of the U1 small nuclear ribonucleoprotein particle (U1 snRNP) are among the most immunogenic molecules in patients with systemic lupus erythematosus and mixed connective tissue disease [49, 50]. A citrullinated peptide panel has been described for the diagnosis of systemic lupus erythematosus using protein microarrays [51].

Taken together, our results highlight PAD2 as a key regulator of inflammation by modulating macrophage polarization. However, the functional roles of the identified novel citrullinated sites in THP-1 macrophages and their involvement in the regulation of the immune response require further study.

Our study has several limitations. We investigated the influence of a pan-PAD inhibitor and PAD2 silencing on THP-1 macrophage polarization. However, we did not perform experiments in which both PAD1 and PAD4 were silenced in parallel with PAD2 to account for the compensatory effects of other PAD in the absence of PAD2.

Conclusions

In summary, our study showed that the expression levels of PAD2, PAD1 and PAD4 were increased in THP-1 macrophages activated to the proinflammatory M1 phenotype and decreased in anti-inflammatory M2 macrophages. We showed that the pan-PAD inhibitor BB-CI-amidine decreased the polarization of THP-1 macrophages to the M1 phenotype and increased activation to the M2 phenotype. This effect was mediated by the downregulation of the NF- κ B pathway. Our

results further showed that silencing PAD increased the polarization of THP-1 macrophages to the M2 phenotype and upregulated proteins related to the antiviral innate immune response and interferon signalling. These results suggested that specifically inhibiting PAD2 could be a novel therapeutic strategy. Importantly, we identified 192 citrullination sites in THP-1 macrophages, and the majority of the citrullinated proteins belong to signalling pathways mediating inflammation, cell death and DNA/RNA processing. However, further investigations are needed to elucidate the exact role of PAD and citrullination in proinflammatory and anti-inflammatory macrophages.

Methods

THP-1 cell culture

The human THP-1 monocytic cell line was obtained from ATCC (Manassas, VA, USA) and grown in a humidified incubator containing 5% CO₂ and 95% air at 37°C in RPMI 1640 medium (Gibco, Waltham, MA, USA) supplemented with 10% foetal bovine serum (FBS, Gibco, Waltham, MA, USA) and streptomycin (100 µg/ml)/penicillin (100 U/ml). To differentiate THP-1 monocytes into macrophages the cells were placed in 6-well plates (1.5 × 10⁶ cells per well) in 3 ml of culture medium and treated with 100 nM phorbol 12-myristate 13-acetate (PMA, Sigma Aldrich, St. Louis, MO, USA) for 48 hrs [52]. After 3 days of rest THP-1 macrophages were polarized for 48 h with 10 ng/ml LPS (*Salmonella Minnesota*; InvivoGen, San Diego, CA, USA) or 20 ng/ml IL-4 (R&D Systems, Minneapolis, MN, USA) to M1 and M2 macrophages, respectively [53]. The control wells were subjected to the same environmental conditions as the stimulated wells. The pan-PAD inhibitor – BB-Cl-amidine (100 nM) was added 30 min before stimulation with LPS or IL-4. The toxicity of BB-Cl-amidine was evaluated by MTT assays at 48 h.

MTT metabolism assay

To assess THP-1-cell viability after 48 h of BB-Cl-amidine treatment, cells were seeded in a 96-well plate at a density of 50,000 cells per well. Then, 10 µL of a 10 mg/ml MTT solution was added to each well and incubated at 37°C for 1 hour. Next, the medium was aspirated, 200 µL of DMSO was added, and the plate was shaken for 1 h to dissolve the dye. The absorbance was measured at 570 nm using a Synergy™ 2 microplate reader (BioTek Instruments Inc., Winooski, VT, USA).

Silencing PAD2

To knockdown PAD2 in THP-1 macrophages, Lipofectamine® RNAiMAX reagent and 25 pmol Silencer® Select PADI2 siRNA (assay ID: s223214) (Thermo Fisher Scientific, Waltham, MA, USA) were used according to the manufacturer's instructions. Silencer® Select Negative Control #2 (assay ID: 4390846) (Thermo Fisher Scientific, Waltham, MA, USA) was used as the scrambled siRNA negative control. Transfection was performed on Day 2 in resting macrophages for 24 h in RPMI 1640 medium without FBS and antibiotics in 6-well plates.

After stimulation, the cell supernatant was collected, passed through 0.22 µm filters and frozen. THP-1 macrophages were lysed in lysis buffer for further experiments.

Quantitative reverse transcription polymerase chain reaction

Activation of THP-1 macrophages to the M1 and M2 phenotypes was determined by real-time PCR. The expression levels of proinflammatory genes (IL-1β, IL-6, TNF-α), anti-inflammatory genes (mannose receptor C-type 1 (MRC1), Fc epsilon receptor II (FCER2), arachidonate 15-lipoxygenase (ALOX15)) and PAD isoforms (PAD1, PAD2, PAD3, PAD4) in THP-1 macrophages were determined according to previously described protocol [54]. Briefly, RNA was isolated using the ReliaPrep™ RNA Cell Miniprep System (Promega, Madison, WI, USA) and transcribed to cDNA with the High Capacity cDNA Reverse Transcription Kit (Thermo Scientific, Waltham, MA, USA). Commercially available primers from Bio-Rad (Hercules, CA, USA) (apart from primers for PAD3: 5'CTGGATTGC GACCTGAACTG3' (forward): 5' TGTGGTCATCAA AGAGGGCT 3' (reverse) and PAD4: 5' ACTCTCCAA GGAACAGAGG 3' (forward), 5' GGTATTCCTTGC CCCTGACT 3' (reverse)) and 2x SsoAdvanced™ Universal SYBR® Green Supermix (Bio-Rad, Hercules, CA, USA) were used for real-time PCR. Analysis of relative gene expression was performed by the CFX96 Touch Real-Time PCR Detection System (Bio-Rad, Hercules, CA, USA) with GAPDH as an internal reference gene, and the data were analysed using the 2^{-ΔΔCt} method in an Excel spreadsheet.

Enzyme-linked immunosorbent assay (ELISA)

The concentrations of proinflammatory cytokines (IL-1β, IL-6, TNF-α) in the supernatant of THP-1 macrophages were measured by a RayBio® Human IL-1 beta ELISA Kit, RayBio® Human IL-6 ELISA Kit and RayBio® Human

TNF-alpha ELISA Kit (RayBiotech, Norcross, GA, USA) according to the manufacturer's instructions.

Seahorse real-time cell metabolic analysis

Mitochondrial respiration in THP-1 macrophages activated to the M1 and M2 phenotypes in the presence of BB-Cl-amidine was measured as the oxygen consumption rate (OCR) using a Seahorse XF96 Metabolic Flux Analyser (Agilent Technologies, Santa Clara, CA, USA). THP-1 monocytes were differentiated into macrophages in Seahorse XF96 cell culture plates at a density of 40,000 cells per well. THP-1 macrophages were stimulated with 10 ng/ml LPS or 20 ng/ml IL-4 in the presence of 100 nM BB-Cl-amidine for 24 h. The Seahorse XF Cell Mito Stress Test was performed according to the manufacturer's protocols. The medium was replaced with XF Base Medium (Agilent, Santa Clara, CA, USA) supplemented with 25 mM glucose, 1 mM sodium pyruvate, and 2 mM L-glutamine (pH 7.4) followed by incubation at 37 °C in a non-CO₂ incubator for 1 hour. Oligomycin (1 μM), carbonyl cyanide phospho-(p)-trifluoromethoxy phenylhydrazone (FCCP) (1 μM), and rotenone/antimycin A (0.5 μM) were subsequently injected into the wells. At the end of the analysis, the medium was removed, and the cells were lysed in RIPA buffer. The protein concentration was measured by the Pierce[™] BCA Protein Assay Kit (Thermo Scientific, Waltham, MA, USA) and used to normalize the OCR. The data were analysed with Wave (version 2.6.1) software (Agilent Technologies, Santa Clara, CA, USA).

Liquid chromatography–tandem MS (LC-MS/MS) analysis of THP-1 macrophages

THP-1 macrophages were lysed in a buffer containing 0.1 M Tris-HCl, pH 7.6, 2% sodium dodecyl sulfate, and 50 mM dithiothreitol (Sigma Aldrich, St. Louis, MO, USA) at 96 °C for 10 min. The protein concentration was determined by a Pierce 660 nm Protein Assay Kit (Thermo Scientific, Waltham, MA, USA). Seventy micrograms of protein was digested overnight using the filter-aided sample preparation (FASP) method [55, 56] with endoproteinase Lys-C (enzyme-to-protein ratio 1:35) as a digestion enzyme. Next, the samples were purified with C18 Ultra-Micro SpinColumns (Harvard Apparatus, Holliston, MA, USA). For macrophage spectral library preparation equal amounts of peptides from all samples were subjected to a high-pH fractionation protocol on C18 Micro SpinColumns (Harvard Apparatus, Holliston, MA). Fractionation was carried out in 50 mM ammonium formate buffer (pH 10) with 12 consecutive elution steps with 5, 10, 12.5, 15, 17.5, 20, 22.5, 25, 27.5, 30, 35 and 50% acetonitrile in 50 mM ammonium formate buffer (pH 10). All samples and library fractions were dissolved

in 0.1% formic acid and 5% acetonitrile at a concentration of 0.5 μg/μl and spiked with the iRT peptides (Biognosys, Schlieren, Switzerland).

One microgram of peptide was injected into a Pep-Map100 RP C18 75 μm i.d. × 25 cm column (Thermo Scientific, Waltham, MA, USA) via a PepMap100 RP C18 75 μm i.d. × 2 cm trap column (Thermo Scientific, Waltham, MA, USA) and separated using a 1 to 40% B phase linear gradient (A phase - 2% ACN and 0.1% FA; B phase - 80% ACN and 0.1% FA) with a flow rate of 300 nL/min on an UltiMate 3000 HPLC system (Thermo Scientific, Waltham, MA, USA) coupled to a TripleTOF 6600+ (Sciex, Framingham, MA, USA) mass spectrometer. The nanoelectrospray ion source (Optiflow, Sciex, Framingham, MA, USA) parameters were as follows: ion spray voltage: 3.2 kV; interface heater temperature (IHT): 200 °C; ion source gas 1 (GS1): 10; and curtain gas (CUR): 25. For DDA acquisition, spectra were collected for 135 min in full scan mode (350–1400 Da), followed by one hundred CID MS/MS scans of one hundred of the most intense precursor ions from the preceding survey full scan exceeding 100 cps intensity under dynamic exclusion criteria. For DIA acquisition, spectra were collected for 100 min in full scan mode (400–1250 Da), followed by one hundred SWATH MS/MS scans using a variable precursor isolation window approach, with m/z windows ranging from 6 to 90 Da.

DDA-MS data were searched against the human UniProt database and MaxQuant Contaminants list using the Pulsar search engine in Spectronaut software (Biognosys, Schlieren, Switzerland) [57] with the following parameters: ± 40 ppm mass tolerance on MS1 and MS2 levels, mutated decoy generation method, Lys-C enzyme specificity, 1% protein and PSM false discovery rate (FDR). The library was generated using 3–6 fragment ions per precursor. The generated human macrophage library was used to analyse DIA-MS data in Spectronaut software. MS data were filtered by 1% FDR at the peptide and protein levels, while quantitation and interference correction were performed at the MS2 level. The data were normalized by a global regression strategy, Q-value percentile data filtering was set at 50%, and global imputation for missing values was performed. Statistical analysis of differential protein abundance was performed at both the MS1 and MS2 levels [58] using unpaired t-tests with multiple testing correction after Storey [59].

Constructing protein-protein interaction (PPI) networks

Functional groupings and pathway analysis were performed using PINE (Protein Interaction Network Extractor) software [60] with the STRING and GeneMANIA databases, a score confidence (0.4) and ClueGO *p* value cut-off < 0.05. The mass spectrometry data have been

deposited to the ProteomeXchange Consortium via the PRIDE partner repository [61] with the dataset identifier PXD034591.

Mapping citrullination sites using a hypercitrullinated library approach

To prepare a hypercitrullinated library, THP-1 macrophages were lysed as described previously. Each sample (200 µg) was divided into two tubes (twin samples). To digest proteins and preserve citrullination residues, the FASP method with Lys-C as the digestion enzyme was used. The deimination reaction was performed on Microcon-30 centrifugal filters during the FASP protocol as described previously [62]. Briefly, one twin sample was treated with the PAD cocktail (cocktail of the five PAD isoforms PAD1, PAD2, PAD3, PAD4, and PAD6; 1:20 ratio, (SignalChem, Richmond, Canada)), while the second sample was treated with H₂O at the same ratio. All samples were incubated in deimination buffer (100 mM Tris-HCl (pH 8.5), 5 mM CaCl₂, 0.5 mM DTT) for 2 h at 37 °C. Then, digestion with Lys-C was carried out overnight at 37 °C, and the samples were cleaned on an Oasis HLB plate (Waters, Milford, MA, USA) prior to LC-MS analysis. To fractionate the desalted samples, a Pierce™ High pH Reversed-Phase Peptide Fractionation Kit (Thermo Fisher Scientific, Waltham, MA, USA) was used according to the manufacturer's instructions with the following modifications: each sample was fractionated into 5 fractions with 7.5, 10, 12.5, 15 and 17.5% ACN in the elution solution. LC-MS analysis was performed as described previously.

A hypercitrullinated library was prepared using SpectraST v.4.0 as described previously [63]. Briefly, all data were searched using X!Tandem Native v.2013.06.15.1, X!Tandem Kscore v.2013.06.15.1, and Comet v.2014.02 rev.2. The search parameters included the following criteria: static modifications of carbamidomethyl (C) and variable modifications of oxidation (M), deamidation (NQ), and citrullination (R). The parent mass tolerance was set at 50 ppm, and the monoisotopic fragment mass tolerance was 100 ppm (which was further filtered to be <0.05 Da to build the spectral library); LysC peptides with up to two missed cleavages were allowed. The identified peptides were processed and analysed by Trans-Proteomic Pipeline v.4.8 and were validated using PeptideProphet scoring, and the PeptideProphet results were statistically refined using iProphet. All peptides were filtered at an FDR of 1% with a peptide probability cut-off of ≥0.99. To identify citrullinated peptides from DIA runs, a hypercitrullinated spectral library generated by SpectraST was used with CitFinder software to analyse modified-unmodified peptide pairs for physicochemical properties such as ΔRT shift, charge state

and neutral loss [63]. Statistical analysis of citrullinated peptides was performed in Perseus [64]. Citrullinated peptide quantities were normalized to their corresponding protein levels. For quantitative analysis, only citrullinated peptides present in at least 50% of each biological group were chosen. Missing values were imputed using a row average imputation method. ANOVA with post-hoc tests and permutation-based FDR correction were used for the statistical analysis of data in Perseus.

Statistical analysis

Variables are expressed as the mean ± SEM. The equality of variance and normality of the data were checked by the Brown-Forsythe test and Shapiro-Wilk test, respectively. Based on the results, statistical analysis was performed using either t test (two groups), ordinary one-way ANOVA, Brown-Forsythe and Welch ANOVA or Kruskal-Wallis tests with correction for multiple comparisons by controlling the False Discovery Rate (two-stage linear step-up procedure of Benjamini, Krieger and Yekutieli) (Graphpad Prism 9.3.1, San Diego, CA, USA). Two-way ANOVA was used for the OCR analysis. Values of *p* < 0.05 (or *q*-values for proteomics experiments) were considered statistically significant.

Abbreviations

ACN: Acetonitrile; AHSG: Alpha-2-HS-glycoprotein (fetuin-A); ALOX15: Arachidonate 15-lipoxygenase; ASC: Apoptosis-associated speck-like protein; BB-Cl: BB-Cl-amidine; BST2: Bone marrow stromal antigen 2; CD74: HLA class II histocompatibility antigen gamma chain; DDA: Data-dependent acquisition; DIA: Data-independent acquisition; EIF2AK2: Double-stranded RNA-activated protein kinase; ETosis: Extracellular trap formation; FA: Formic acid; FASP: Filter-aided sample preparation; FC: Fold change; FCER2: Fc epsilon receptor II; FDR: False discovery rate; IFI35: Interferon-induced 35 kDa protein; IFITM3: Interferon-induced transmembrane protein 3; IFN-γ: Interferon gamma; IKKβ: NF-κappa-B essential modulator; IKK2: Inhibitor of nuclear factor kappa-B kinase subunit beta; IL: Interleukin; ISG15: Ubiquitin-like protein ISG15; LC-MS/MS: Liquid chromatography – tandem mass spectrometry; LPS: Lipopolysaccharide; MAVS: Mitochondrial antiviral-signalling protein; MIF: Macrophage migration inhibitory factor; MRC1: Mannose receptor C-type 1; MS: Mass spectrometry; MX1/2: Interferon-induced GTP-binding protein Mx1/Mx2; NO: Nitric oxide; OAS1/2/3: 2'-5'-oligoadenylate synthase 1/2/3; OCR: Oxygen consumption rate; PAD: Protein arginine deiminase; PINE: Protein interaction network extractor; PMA: Phorbol 12-myristate 13-acetate; PRKCB: Protein kinase C beta type; PTM: Posttranslational modification; RIG-I: Antiviral innate immune response receptor RIG-I; RIPK1: Receptor-interacting serine/threonine-protein kinase 1; siCON: Scrambled siRNA control; siPAD2: Silenced PAD2; SNRPD2: Small nuclear ribonucleoprotein Sm D2; STING1: Stimulator of interferon genes protein; TNF-α: Tumour necrosis factor α; TXNIP: Thioredoxin-interacting protein; UBE2V1: ubiquitin-conjugating enzyme E2 variant 1; XRCC6: X-ray repair cross-complementing protein 6 (Ku70).

Supplementary Information

The online version contains supplementary material available at <https://doi.org/10.1186/s12950-022-00317-8>.

Additional file 1: Supplemental Figure 1. Quality control of MS runs of THP-1 macrophages activated to M1 and M2 phenotype in the presence of pan-PAD inhibitor - BB-Cl. A) Total ion chromatogram (TIC) overlay of all LC-MS runs showed excellent separation reproducibility. B) Protein group

identification details across all LC-MS runs. C) Spectral library recovery. D) Coefficient of variations for protein groups across experimental conditions.

Supplemental Figure 2. Bioinformatic functional network analysis of THP-1 macrophages activated to proinflammatory and anti-inflammatory phenotype. A) Enriched functional network generated by PINE (Protein Interaction Network Extractor) in THP-1 macrophages treated with LPS in comparison to control. B) Enriched functional network generated by PINE (Protein Interaction Network Extractor) in THP-1 macrophages treated with IL-4 in comparison to control. Activated pathways are shown as orange central nodes and inhibited pathways are shown as blue central nodes along with red (upregulated) or blue (downregulated) protein nodes. **Supplemental Figure 3.** Quality control of MS runs of THP-1 macrophages with PAD2 knockout activated to M1 phenotype. A) Total ion chromatogram (TIC) overlay of all LC-MS runs showed excellent separation reproducibility. B) Protein group identification details across all LC-MS runs. C) Spectral library recovery. D) Coefficient of variations for protein groups across experimental conditions.

Additional file 2: Supplemental Table 1 A. Differentially expressed proteins in THP-1 macrophages treated with BB-Cl-amidine as compared to control group ($q < 0.05$, $n = 5$). **Supplemental Table 1 B.** Differentially expressed proteins in THP-1 macrophages treated with LPS as compared to control group ($q < 0.05$, $n = 5$). **Supplemental Table 1 C.** Differentially expressed proteins in THP-1 macrophages treated with IL-4 as compared to control group ($q < 0.05$, $n = 5$). **Supplemental Table 1 D.** Differentially expressed proteins in THP-1 macrophages treated with LPS and BB-Cl-amidine as compared to LPS group ($q < 0.05$, $n = 5$). **Supplemental Table 1 E.** Differentially expressed proteins in THP-1 macrophages treated with IL-4 and BB-Cl-amidine as compared to IL-4 group ($q < 0.05$, $n = 5$).

Additional file 3: Supplemental Table 2 A. Differentially expressed proteins in THP-1 macrophages with silenced PAD2 as compared to scrambled siRNA control group ($q < 0.05$, $n = 6$). **Supplemental Table 2 B.** Differentially expressed proteins in THP-1 macrophages with silenced PAD2 and treated with LPS as compared to scrambled siRNA control group treated with LPS ($q < 0.05$, $n = 6$).

Additional file 4: Supplemental Table 3 A. All citrullinated peptides quantified in THP-1 macrophages polarized to M1 and M2 phenotype in the presence of BB-Cl-amidine. **Supplemental Table 3 B.** All citrullinated peptides quantified in LPS stimulated THP-1 macrophages with silenced PAD2.

Acknowledgements

Not applicable.

Authors' contributions

AS and JFB were responsible for the conception and design of the study. AS, RP, VV, and NS were responsible for analyses of the samples. AS and JFB were responsible for interpretation of the data. AS, JFB, and JVE drafted the article. All authors revised the paper critically for important intellectual content and gave final approval of the version to be published.

Funding

This research was supported by the National Science Centre (NCN) (grant number 2017/26/D/NZ4/00480) and the Polish National Agency for Academic Exchange (NAWA).

Availability of data and materials

The proteomic datasets generated during the current study are available in the ProteomeXchange Consortium via the PRIDE partner repository with the dataset identifier PXD034591.

The other datasets used and/or analysed during the current study are available from the corresponding author on reasonable request.

Declarations

Ethics approval and consent to participate

Not applicable.

Consent for publication

Not applicable.

Competing interests

The authors declare that they have no competing interests.

Author details

¹Chair of Pharmacology, Jagiellonian University Medical College, Krakow, Poland. ²Advanced Clinical Biosystems Research Institute, Smidt Heart Institute, Cedars-Sinai Medical Center, CA, Los Angeles, USA. ³Advanced Clinical Biosystems Research Institute, Precision Biomarker Laboratories, Cedars-Sinai Medical Center, Los Angeles, CA, USA.

Received: 30 June 2022 Accepted: 31 October 2022

Published online: 18 November 2022

References

- György B, Tóth E, Tarcsa E, Falus A, Buzás EI. Citrullination: a posttranslational modification in health and disease. *Int J Biochem Cell Biol.* 2006;38:1662–77.
- Amin B, Voelter W. Human deiminases: isoforms, substrate specificities, kinetics, and detection. *Prog Chem Org Nat Prod.* 2017;106:203–40.
- Alghamdi M, Alasmari D, Assiri A, Mattar E, Aljaddawi AA, Alattas SG, et al. An overview of the intrinsic role of Citrullination in autoimmune disorders. *J Immunol Res.* 2019;2019:7592851.
- Witalison EE, Thompson PR, Hofseth LJ. Protein arginine deiminases and associated Citrullination: physiological functions and diseases associated with dysregulation. *Curr Drug Targets.* 2015;16:700–10.
- Knight JS, Subramanian V, O'Dell AA, Yalavarthi S, Zhao W, Smith CK, et al. Peptidylarginine deiminase inhibition disrupts NET formation and protects against kidney, skin and vascular disease in lupus-prone MRL/lpr mice. *Ann Rheum Dis.* 2015;74:2199–206.
- Yu H-C, Tung C-H, Huang K-Y, Huang H-B, Lu M-C. The essential role of Peptidylarginine deiminases 2 for cytokines secretion, apoptosis, and cell adhesion in macrophage. *Int J Mol Sci.* 2020;21:E5720.
- Tatsiy O, McDonald PP. Physiological stimuli induce PAD4-dependent, ROS-independent NETosis, with early and late events controlled by discrete signaling pathways. *Front Immunol.* 2018;9 Available from: <https://www.frontiersin.org/article/10.3389/fimmu.2018.02036>. Cited 2022 May 27.
- Mohan S, Horibata S, McElwee JL, Dannenberg AJ, Coonrod SA. Identification of macrophage extracellular trap-like structures in mammary gland adipose tissue: a preliminary study. *Front Immunol.* 2013;4:67.
- Mishra N, Schwerdtner L, Sams K, Mondal S, Ahmad F, Schmidt RE, et al. Cutting edge: protein arginine deiminase 2 and 4 regulate NLRP3 Inflammasome-dependent IL-1 β maturation and ASC speck formation in macrophages. *J Immunol Baltim Md.* 1950;2019(203):795–800.
- Hojo-Nakashima I, Sato R, Nakashima K, Hagiwara T, Yamada M. Dynamic expression of peptidylarginine deiminase 2 in human monocytic leukaemia THP-1 cells during macrophage differentiation. *J Biochem (Tokyo).* 2009;146:471–9.
- Xu H, Jiang J, Chen W, Li W, Chen Z. Vascular macrophages in atherosclerosis. *J Immunol Res.* 2019;2019:4354786.
- Siouti E, Andreacos E. The many facets of macrophages in rheumatoid arthritis. *Biochem Pharmacol.* 2019;165:152–69.
- Mammana S, Fagone P, Cavalli E, Basile MS, Petralia MC, Nicoletti F, et al. The role of macrophages in Neuroinflammatory and neurodegenerative pathways of Alzheimer's disease, amyotrophic lateral sclerosis, and multiple sclerosis: Pathogenetic cellular effectors and potential therapeutic targets. *Int J Mol Sci.* 2018;19:831.
- Gordon S. Alternative activation of macrophages. *Nat Rev Immunol Nature Publishing Group.* 2003;3:23–35.
- Mosser DM, Edwards JP. Exploring the full spectrum of macrophage activation. *Nat Rev Immunol.* 2008;8:958–69.
- Chawla A. Control of macrophage activation and function by PPARs. *Circ Res.* 2010;106:1559–69.
- Parisi L, Gini E, Baci D, Tremolati M, Fanuli M, Bassani B, et al. Macrophage polarization in chronic inflammatory diseases: killers or builders? *J Immunol Res.* 2018;2018:8917804.

18. Luo Y, Arita K, Bhatia M, Knuckley B, Lee Y-H, Stallcup MR, et al. Inhibitors and Inactivators of protein arginine deiminase 4: functional and structural characterization. *Biochemistry*. 2006;45:11727–36.
19. Wu C-J, Conze DB, Li T, Srinivasula SM, Ashwell JD. Sensing of Lys 63-linked polyubiquitination by NEMO is a key event in NF- κ B activation [corrected]. *Nat Cell Biol*. 2006;8:398–406.
20. Saijo K, Mecklenbräuker I, Santana A, Leitger M, Schmedt C, Tarakhovskiy A. Protein kinase C β controls nuclear factor κ B activation in B cells through selective regulation of the I κ B kinase α . *J Exp Med*. 2002;195:1647–52.
21. Salmerón A, Janzen J, Soneji Y, Bump N, Kamens J, Allen H, et al. Direct phosphorylation of NF- κ B1 p105 by the I κ B kinase complex on serine 927 is essential for signal-induced p105 proteolysis. *J Biol Chem*. 2001;276:22215–22.
22. Deng L, Wang C, Spencer E, Yang L, Braun A, You J, et al. Activation of the I κ B kinase complex by TRAF6 requires a dimeric ubiquitin-conjugating enzyme complex and a unique polyubiquitin chain. *Cell*. 2000;103:351–61.
23. Xiahou Z, Wang X, Shen J, Zhu X, Xu F, Hu R, et al. NMI and IFP35 serve as proinflammatory DAMPs during cellular infection and injury. *Nat Commun*. 2017;8:950.
24. Seth RB, Sun L, Ea C-K, Chen ZJ. Identification and characterization of MAVS, a mitochondrial antiviral signaling protein that activates NF- κ B and IRF 3. *Cell*. 2005;122:669–82.
25. Bonnet MC, Weil R, Dam E, Hovanessian AG, Meurs EF. PKR stimulates NF- κ B irrespective of its kinase function by interacting with the I κ B kinase complex. *Mol Cell Biol*. 2000;20:4532–42.
26. Cho YS, Challa S, Moquin D, Genga R, Ray TD, Guildford M, et al. Phosphorylation-driven assembly of the RIP1-RIP3 complex regulates programmed necrosis and virus-induced inflammation. *Cell*. 2009;137:1112–23.
27. Tak PP, Firestein GS. NF- κ B: a key role in inflammatory diseases. *J Clin Invest Am Soc Clin Investig*. 2001;107:7–11.
28. Liu T, Zhang L, Joo D, Sun S-C. NF- κ B signaling in inflammation. *Signal Transduct Target Ther*. 2017;2:17023.
29. Tao P, Sun J, Wu Z, Wang S, Wang J, Li W, et al. A dominant autoinflammatory disease caused by non-cleavable variants of RIPK1. *Nature*. 2020;577:109–14.
30. Ishikawa H, Ma Z, Barber GN. STING regulates intracellular DNA-mediated, type I interferon-dependent innate immunity. *Nature*. 2009;461:788–92.
31. Gomes MTR, Guimarães ES, Marinho FV, Macedo I, Aguiar ERGR, Barber GN, et al. STING regulates metabolic reprogramming in macrophages via HIF-1 α during Brucella infection. *PLoS Pathog*. 2021;17:e1009597.
32. Li Y, Gu C, Liu G, Yu Y, Xu J. Polarization of rheumatoid macrophages is regulated by the CDKN2B-AS1/ MIR497/TXNIP axis. *Immunol Lett*. 2021;239:23–31.
33. Wang Y, Ning X, Gao P, Wu S, Sha M, Lv M, et al. Inflammasome activation triggers Caspase-1-mediated cleavage of cGAS to regulate responses to DNA virus infection. *Immunity*. 2017;46:393–404.
34. Lee HJ, Joo M, Abdolrasulnia R, Young DG, Choi I, Ware LB, et al. Peptidylarginine deiminase 2 suppresses inhibitory (κ)B kinase activity in lipopolysaccharide-stimulated RAW 264.7 macrophages. *J Biol Chem*. 2010;285:39655–62.
35. Liu Q, Imaizumi T, Aizawa T, Hirono K, Kawaguchi S, Watanabe S, et al. Cytosolic sensors of viral RNA are involved in the production of Interleukin-6 via toll-like receptor 3 signaling in human glomerular endothelial cells. *Kidney Blood Press Res*. 2019;44:62–71.
36. Cai J, Huang L, Tang H, Xu H, Wang L, Zheng M, et al. Macrophage migration inhibitory factor of *Thelazia callipaeda* induces M2-like macrophage polarization through TLR4-mediated activation of the PI3K-Akt pathway. *FASEB J Off Publ Fed Am Soc Exp Biol*. 2021;35:e21866.
37. Ghoochani A, Schwarz MA, Yakubov E, Engelhorn T, Doerfler A, Buchfelder M, et al. MIF-CD74 signaling impedes microglial M1 polarization and facilitates brain tumorigenesis. *Oncogene*. 2016;35:6246–61.
38. de Souza B, Rizzo M, Brasilino de Carvalho M, Kim EJ, Rendon BE, Noe JT, et al. Oral squamous carcinoma cells promote macrophage polarization in an MIF-dependent manner. *QJM Mon J Assoc Phys*. 2018;111:769–78.
39. Cotzomi-Ortega I, Nieto-Yañez O, Juárez-Avelar I, Rojas-Sanchez G, Montes-Alvarado JB, Reyes-Leyva J, et al. Autophagy inhibition in breast cancer cells induces ROS-mediated MIF expression and M1 macrophage polarization. *Cell Signal*. 2021;86:110075.
40. Morchikh M, Cribier A, Raffel R, Amraoui S, Cau J, Severac D, et al. HEXIM1 and NEAT1 long non-coding RNA form a multi-subunit complex that regulates DNA-mediated innate immune response. *Mol Cell*. 2017;67:387–399.e5.
41. Sun H, Li Q, Yin G, Ding X, Xie J. Ku70 and Ku80 participate in LPS-induced pro-inflammatory cytokines production in human macrophages and monocytes. *Aging*. 2020;12:20432–44.
42. Wiche G. Plectin-mediated intermediate filament functions: why isoforms matter. *Cells*. 2021;10:2154.
43. Sipilä K, Haag S, Denessiouk K, Käpylä J, Peters EC, Denesyuk A, et al. Citrullination of collagen II affects integrin-mediated cell adhesion in a receptor-specific manner. *FASEB J Off Publ Fed Am Soc Exp Biol*. 2014;28:3758–68.
44. Li FJ, Suroli R, Li H, Wang Z, Liu G, Kulkarni T, et al. Citrullinated vimentin mediates development and progression of lung fibrosis. *Sci Transl Med*. 2021;13:eaba2927.
45. Chatterjee P, Seal S, Mukherjee S, Kundu R, Mukherjee S, Ray S, et al. Adipocyte fetuin-a contributes to macrophage migration into adipose tissue and polarization of macrophages. *J Biol Chem*. 2013;288:28324–30.
46. Rudloff S, Jahnhen-Dechent W, Huynh-Do U. Tissue chaperoning—the expanded functions of fetuin-A beyond inhibition of systemic calcification. *Pflüg Arch - Eur J Physiol*. 2022. Cited 2022 Jun 9; Available from: <https://doi.org/10.1007/s00424-022-02688-6>.
47. Tekeoğlu İ, Harman H, Sağ S, Altındiş M, Kamanlı A, Nas K. Levels of serum pentraxin 3, IL-6, fetuin a and insulin in patients with rheumatoid arthritis. *Cytokine*. 2016;83:171–5.
48. Ishikawa H, Nobe Y, Izumikawa K, Yoshikawa H, Miyazawa N, Terukina G, et al. Identification of truncated forms of U1 snRNA reveals a novel RNA degradation pathway during snRNP biogenesis. *Nucleic Acids Res*. 2014;42:2708–24.
49. van Venrooij WJ. Autoantibodies against small nuclear ribonucleoprotein components. *J Rheumatol Suppl*. 1987;14(Suppl 13):78–82.
50. Somarelli JA, Mesa A, Rodriguez R, Avellan R, Martinez L, Zang YJ, et al. Epitope mapping of the U1 small nuclear ribonucleoprotein particle in patients with systemic lupus erythematosus and mixed connective tissue disease. *Lupus*. 2011;20:274–89.
51. Wang Y, Liu H, Fu Y, Kao W, Ji Y, Liu X, et al. Novel biomarkers containing citrullinated peptides for diagnosis of systemic lupus erythematosus using protein microarrays. *Clin Exp Rheumatol*. 2019;37:929–36.
52. Chanput W, Mes JJ, Wichers HJ. THP-1 cell line: an in vitro cell model for immune modulation approach. *Int Immunopharmacol*. 2014;23:37–45.
53. Baxter EW, Graham AE, Re NA, Carr IM, Robinson JI, Mackie SL, et al. Standardized protocols for differentiation of THP-1 cells to macrophages with distinct M (IFN γ +LPS), M (IL-4) and M (IL-10) phenotypes. *J Immunol Methods*. 2020;478:112721.
54. Stachowicz A, Olszanecki R, Suski M, Wiśniewska A, Totorń-Żurańska J, Madej J, et al. Mitochondrial aldehyde dehydrogenase activation by alda-1 inhibits atherosclerosis and attenuates hepatic steatosis in apolipoprotein e-knockout mice. *J Am Heart Assoc*. 2014;3(6):e001329. <https://doi.org/10.1161/JAHA.114.001329>.
55. Wiśniewski JR, Zougman A, Mann M. Combination of FASP and StageTip-based fractionation allows in-depth analysis of the hippocampal membrane proteome. *J Proteome Res*. 2009;8:5674–8.
56. Wiśniewski JR, Rakus D. Multi-enzyme digestion FASP and the ‘Total protein approach’-based absolute quantification of the *Escherichia coli* proteome. *J Proteome*. 2014;109:322–31.
57. Bruderer R, Bernhardt OM, Gandhi T, Miladinović SM, Cheng L-Y, Messner S, et al. Extending the limits of quantitative proteome profiling with data-independent acquisition and application to acetaminophen-treated three-dimensional liver microtissues. *Mol Cell Proteomics MCP*. 2015;14:1400–10.
58. Huang T, Bruderer R, Muntel J, Xuan Y, Vitek O, Reiter L. Combining precursor and fragment information for improved detection of differential abundance in data independent acquisition. *Mol Cell Proteomics MCP*. 2020;19:421–30.
59. Storey JD. A direct approach to false discovery rates. *J R Stat Soc Ser B Stat Methodol*. 2002;64:479–98.
60. Sundararaman N, Go J, Robinson AE, Mato JM, Lu SC, Van Eyk JE, et al. PINE: an automation tool to extract and visualize protein-centric functional networks. *J Am Soc Mass Spectrom*. 2020;31:1410–21.

61. Vizcaíno JA, Deutsch EW, Wang R, Csordas A, Reisinger F, Ríos D, et al. ProteomeXchange provides globally coordinated proteomics data submission and dissemination. *Nat Biotechnol.* 2014;32:223–6.
62. Stachowicz A, Sundararaman N, Venkatraman V, Van Eyk J, Fert-Bober J. pH/acetonitrile-gradient reversed-phase fractionation of enriched hyper-Citrullinated library in combination with LC-MS/MS analysis for confident identification of Citrullinated peptides. *Methods Mol Biol Clifton NJ.* 2022;2420:107–26.
63. Fert-Bober J, Venkatraman V, Hunter CL, Liu R, Crowgey EL, Pandey R, et al. Mapping Citrullinated sites in multiple organs of mice using Hypercitrullinated library. *J Proteome Res.* 2019;18:2270–8.
64. Tyanova S, Temu T, Sinitcyn P, Carlson A, Hein MY, Geiger T, et al. The Perseus computational platform for comprehensive analysis of (prote) omics data. *Nat Methods.* 2016;13:731–40.

Publisher's Note

Springer Nature remains neutral with regard to jurisdictional claims in published maps and institutional affiliations.

Ready to submit your research? Choose BMC and benefit from:

- fast, convenient online submission
- thorough peer review by experienced researchers in your field
- rapid publication on acceptance
- support for research data, including large and complex data types
- gold Open Access which fosters wider collaboration and increased citations
- maximum visibility for your research: over 100M website views per year

At BMC, research is always in progress.

Learn more biomedcentral.com/submissions

